Physics of the Solid State, Vol. 47, No. 3, 2005, pp. 489–494. Translated from Fizika Tverdogo Tela, Vol. 47, No. 3, 2005, pp. 474–479.

MAGNETISM AND FERROELECTRICITY

Optical Properties and Electronic Structure of Rare-Earth Ferroborates

V. N. Zabluda, S. G. Ovchinnikov, A. M. Potseluĭko, and S. A. Kharlamova

Kirensky Institute of Physics, Siberian Division, Russian Academy of Sciences, Akademgorodok, Krasnoyarsk, 660036 Russia

e-mail: stais@iph.krasn.ru, sgo@iph.krasn.ru

Received May 17, 2004

Abstract—The optical absorption spectra of single-crystal ferroborate $GdFe_3(BO_3)_4$ and $GdFe_{2.1}Ga_{0.9}(BO_3)_4$ are measured and interpreted. It is found that the absorption edge and the absorption bands *A*, *B*, and *C* observed below the edge are close to those for $FeBO_3$. A many-electron model of the band structure of $GdFe_3(BO_3)_4$ is suggested including strong electron correlations between the iron *d* states. It is shown that $GdFe_3(BO_3)_4$ has a charge-transfer dielectric gap. A rise in pressure is predicted to result in a crossover between the high-spin and low-spin states of the Fe^{3+} ion, collapse of the magnetic moment, a weakening of Coulomb correlations, an abrupt reduction in the energy gap, and an insulator–semiconductor transition. *© 2005 Pleiades Publishing, Inc.*

1. INTRODUCTION

For more than 30 years, studies of the rare-earth oxiborates with the huntite structure $RM_3(BO_3)_4$ have been carried out in order to fabricate high-efficiency functional materials for laser, piezoelectric, and acoustic devices. These crystals, along with the high-temperature superconductor cuprates and manganites exhibiting colossal magnetoresistance, are examples of systems with strong electron correlation (SEC). SEC determines their electronic structure and magnetic, optical, and electrical properties.

The rare-earth ferroborate $GdFe_3(BO_3)_4$ has the huntite structure belonging to space group $R32(D_{3h}^7)$, with $Z = 3$. The rare-earth Gd^{3+} ions have a prismatic environment, and the Fe^{3+} ions have an octahedral environment [1]. $GdFe_3(BO_3)_4$ is known to be an easy-plane antiferromagnet with a Néel temperature $T_N = 38$ K [2, 3]. At 10 K, all the sublattices are subjected to the spin-flop reorientation transition into the easy-axis antiferromagnetic (AFM) phase. This material is an insulator at room temperature.

Of the entire collection of oxiborates of transition metals, $FeBO_3$ ferroborate is the most interesting and most similar for comparison with the single-crystal $GdFe_3(BO_3)_4$ studied in the present work. This compound has been studied for a long time, and its magnetic [4, 5], optical [6], and dielectric properties are well known. Recently, optically induced disordering of the magnetic order was observed to occur in this compound under pulsed optical pumping [7]. At normal pressure, this material is a charge-transfer insulator with an optical gap of 2.9 eV [6, 8]. $FeBO_3$ is a typical representative of the systems with SEC [9]. Recent studies of this compound under high pressure have shown dramatic changes in its magnetic and electrical properties associated with the insulator–semiconductor transition [10–12].

This work is devoted to the optical absorption spectra and the electronic structure of $GdFe_3(BO_3)_4$, which have not yet been studied. Section 2 describes the specimens and experimental techniques used. In Section 3, we present the measured optical absorption spectra of $GdFe_3(BO_3)_4$ and $GdFe_{2.1}Ga_{0.9}(BO_3)_4$. In Section 4, the optical properties are analyzed in the terms of the multiband model of the electronic structure of $GdFe_3(BO_3)_4$ and are compared with those of $FeBO_3$. Section 5 is concerned with predictions of the influence of an increase in pressure on the optical properties and electronic structure.

2. SPECIMENS AND EXPERIMENTAL TECHNIQUE

$GdFe_3(BO_3)_4$ and $GdFe_{2.1}Ga_{0.9}(BO_3)_4$ single crystals were grown from a solution in melt using the group technique with a seed [13]. The obtained single crystals were dark green ($GdFe_3(BO_3)_4$), green ($GdFe_{2.1}Ga_{0.9}(BO_3)_4$), or transparent in the visible region. To carry out optical measurements, specimens from bulk isometric crystals were prepared in the form of thin plates with their planes either parallel or normal to the threefold axis C_3. The thickness of the plates intended for optical measurements was about 53 μm for the first crystallographic orientation of plates and about 42(37) μm for the second orientation, with the area of plates in both cases being about 2 mm^2. The spectra of optical absorption $D = \ln(I_0/I)$ for both $GdFe_3(BO_3)_4$ and $GdFe_{2.1}Ga_{0.9}(BO_3)_4$ were obtained using a double-beam spectrometer (designed at the Institute of Physics,

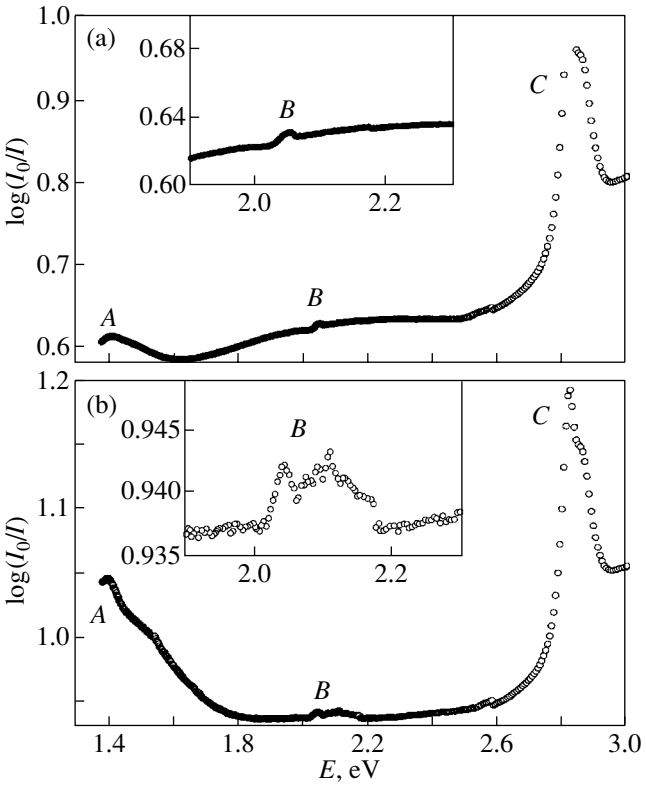

Fig. 1. Optical absorption spectra at T = 300 K for (a) $GdFe_3(BO_3)_4$ and (b) $GdFe_{2.1}Ga_{0.9}(BO_3)_4$.

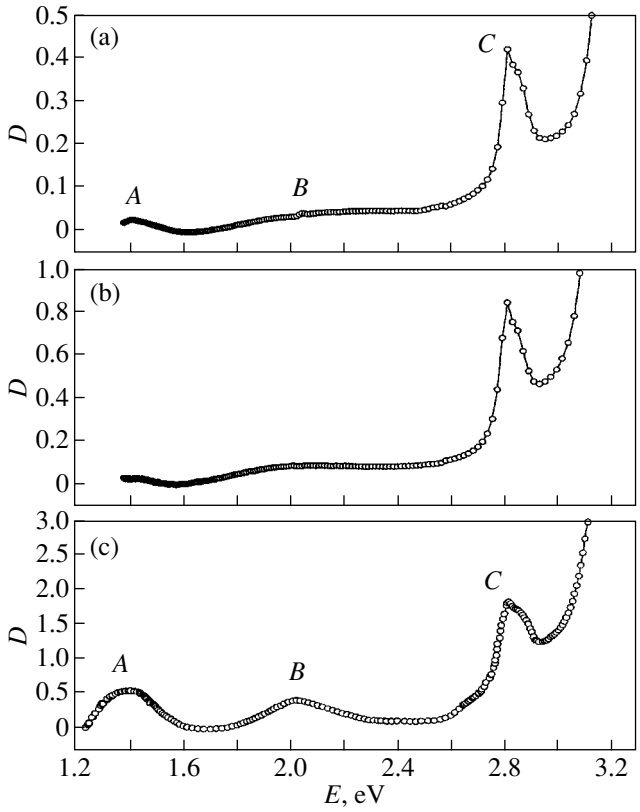

Fig. 2. Optical absorption spectra (a, b) of $GdFe_3(BO_3)_4$ for the *c* and *a* directions, respectively, and (c) of $FeBO_3$.

Siberian Division, Russian Academy of Sciences) in the range 10000–40000 cm^{-1} (1.24–4.96 eV) at 300 K. The slit spectral width of the grating monochromator used was 10 cm^{-1}. The absorption was measured with an accuracy of 3%.

3. OPTICAL ABSORPTION SPECTRA OF $GdFe_3(BO_3)_4$ AND $GdFe_{2.1}Ga_{0.9}(BO_3)_4$

The measured optical absorption spectra of $GdFe_3(BO_3)_4$ and $GdFe_{2.1}Ga_{0.9}(BO_3)_4$ are shown in Fig. 1. In the spectrum of $GdFe_{2.1}Ga_{0.9}(BO_3)_4$, the *B* peak is clearly observed to split. In Fig. 2, the $GdFe_3(BO_3)_4$ absorption spectra for two directions of the incident light beam with respect to the crystallographic C_3 axis are shown in comparison with the spectrum of the well-known compound $FeBO_3$ [6, 8].

B–O and Fe–O lengths and the energy gaps in $FeBO_3$ and $GdFe_3(BO_3)_4$

	B–O, Å	Fe–O, Å	E_g, eV
$FeBO_3$	1.3790	2.028	2.9
$GdFe_3(BO_3)_4$	1.3676	2.029	3.1

The energy band gap, which determines the fundamental absorption edge in $GdFe_3(BO_3)_4$, is equal to E_g = 3.1 eV, which is slightly higher than the corresponding value in $FeBO_3$ (E_g = 2.9 eV). Three groups of bands were observed (at E = 1.4, 2.0, 2.8 eV), which were the same for both crystallographic orientations. It was found that the bands in the spectra of $GdFe_3(BO_3)_4$ and $FeBO_3$ have similar energies to within an accuracy of several tenths of an electronvolt. Based on this similarity, we assumed that the optical properties of $FeBO_3$ and $GdFe_3(BO_3)_4$ are identical in the range 1.0–3.5 eV.

The influence of the rare-earth Gd^{3+} ion on the optical spectrum was clarified by studying high-resolution Fourier spectra. It was established that the Gd^{3+} ion does not have any fundamental absorption bands up to 32264 cm^{-1} (4 eV) [14]; therefore, the *A*, *B*, *C* bands can be associated with absorption of Fe^{3+} ions. Thus, all transitions are related to the Fe^{3+} ion and its nearest environment.

The difference between the local crystal structures of $GdFe_3(BO_3)_4$ and $FeBO_3$ is as follows: the single-crystal $GdFe_3(BO_3)_4$, unlike $FeBO_3$, has a slightly distorted coordination oxygen octahedron FeO_6 and three pairs of equal Fe–O lengths that are fairly close in value (the table shows the mean lengths for $GdFe_3(BO_3)_4$).

Therefore, along with the cubic component, the crystal field also has a low-symmetry component. However, this component is small and we will neglect it in our further discussion.

Thus, the band groups *A*, *B*, and *C* observed in $GdFe_3(BO_3)_4$ (as well as in $FeBO_3$; Fig. 2c) can be interpreted as *d–d* transitions from the ground state of iron ions with spin $S = 5/2$ to an excited state with spin $S = 3/2$, more specifically, ${}^6A_{1g}({}^6S) \longrightarrow {}^4T_{1g}({}^4G)$ for the *A* group of bands, ${}^6A_{1g}({}^6S) \longrightarrow {}^4T_{2g}({}^4G)$ for the *B* group, and ${}^6A_{1g}({}^6S) \longrightarrow {}^4A_{1g}, {}^4E_g({}^4G)$ for the *C* group. Furthermore, the Fe–O and B–O lengths (see table) for $GdFe_3(BO_3)_4$ and for $FeBO_3$ are virtually identical, which allows one to infer that the electronic structures of these two crystals are similar in the energy range up to 4 eV in the vicinity of the Fermi level.

4. ANALYSIS OF THE OPTICAL PROPERTIES OF $GdFe_3(BO_3)_4$ IN TERMS OF A MULTIELECTRON MODEL OF THE BAND STRUCTURE OF OXIBORATES: COMPARISON WITH $FeBO_3$

This section contains an analysis of the properties of $GdFe_3(BO_3)_4$ in the terms of the multielectron model used in [15] to calculate the $FeBO_3$ band structure. This model is also valid for $GdFe_3(BO_3)_4$ in the energy range up to 4 eV.

In insulator $GdFe_3(BO_3)_4$, there are localized Fe^{3+} *d* electrons in FeO_6 octahedra and localized Gd^{3+} *f* electrons in the GdO_6 triangle prism. Within the BO_3 group, strong *sp* hybridization occurs between the boron and oxygen orbitals. According to calculations of the $FeBO_3$ band structure, the hybridization of the Fe *d* electrons with the *sp* electrons of the BO_3 group is negligibly small. The top of the filled valence band E_v and the bottom of the empty conduction band E_c are formed by the *sp* orbitals of the BO_3 group, which, therefore, determine the band gap $E_g = E_c - E_v$.

According to one-electron first-principles calculations, in the case where the Fe^{3+} d^5 terms and Gd^{3+} f^7 terms are partly occupied, there will be partly filled bands, which corresponds to the metal state. However, owing to SEC, both the *d* and *f* electrons are in the Mott–Hubbard insulator regime. Therefore, in order to adequately describe the electronic structure and the optical properties of $GdFe_3(BO_3)_4$, the multielectron approach should be used with inclusion of SEC. Since the bond lengths within the BO_3 group are close to the corresponding lengths in $FeBO_3$ (see table), we can assume that the band gaps $E_g = E_c - E_v$ are also similar for these crystals. A certain decrease in the B–O bond length in $GdFe_3(BO_3)_4$ results in strengthening of the B–O hybridization and in E_g increasing to 3.1 eV as compared to 2.9 eV in $FeBO_3$. The one-electron scheme of the valence and conduction bands is superimposed by one-particle *d*- and *f*-electron resonances at energies

$$\Omega_d = E(d^{n+1}) - E(d^n), \quad \Omega_f = E(f^{n+1}) - E(f^n), \tag{1}$$

where $E(d^n)$ and $E(f^n)$ are the energies of the many-electron terms of iron and gadolinium. These energies are calculated with inclusion of SEC effects. Since Fe–O and Gd–O hybridization is weak, the Ω levels interact with *sp* bands of the BO_3 group only weakly.

The absence of absorption for the Gd^{3+} ion within the energy range $\hbar\omega \le 4$ eV indicates that the filled level $\Omega_{fv} = E(f^7) - E(f^6)$ is very low, while the empty level $\Omega_{fc} = E(f^8) - E(f^7)$ is very high. Therefore, only iron *d* states fall into the band gap E_g and we can conclude that the electronic structures of $FeBO_3$ and $GdFe_3(BO_3)_4$ in the energy range studied are similar. Moreover, because the Fe–O lengths of the FeO_6 octahedra are similar in $FeBO_3$ and in $GdFe_3(BO_3)_4$, we may also expect that the same will be true for both the Racah parameters *A*, *B*, and *C* and the cubic crystal-field component $\Delta = \varepsilon_d(e_g) - \varepsilon_d(t_{2g})$ for the iron ion. Taking SEC into account, the energies of the fundamental terms of the d^n configurations can be expressed in terms of these parameters as follows [15, 16]:

$$\begin{aligned} E({}^5E_1, d^4) &= 4\varepsilon_d + 6A - 21B - 0.6\Delta, \\ E({}^6A_1, d^5) &= 5\varepsilon_d + 10A - 35B, \\ E({}^5T_2, d^6) &= 6\varepsilon_d + 15A - 21B - 0.4\Delta. \end{aligned} \tag{2}$$

Here, ε_d is the one-electron energy of a *d* electron in the atom. In the cubic crystal field, this level splits: $\varepsilon_d(t_{2g}) = \varepsilon_d - 0.4\Delta$ and $\varepsilon_d(e_g) = \varepsilon_d + 0.6\Delta$. The Racah parameters and the crystal field depend on the number of *d* electrons in the d^n configuration; however, this dependence is weak and we neglect it for the sake of simplicity. In the $GdFe_3(BO_3)_4$ compound, as in $FeBO_3$, the *d–d* transitions in Fe^{3+} with the energies

$$\begin{aligned} \varepsilon_A = E({}^4T_1) - E({}^6A_1), \quad \varepsilon_B = E({}^4T_2) - E({}^6A_1), \\ \varepsilon_C = E({}^4E_1) - E({}^6A_1) \end{aligned} \tag{3}$$

determine the absorption spectrum at $\hbar\omega < E_g$. Using the experimental energies of *d–d* transitions and the Tanabe–Sugano diagrams, the Racah parameters are determined to be $B = 0.084$ eV, $C = 0.39$ eV, and $\Delta = 1.57$ eV; these parameters are similar to the Racah parameters for $FeBO_3$. The parameter *A* and the one-electron energies ε_d are determined by the Fe^{3+} ion and are taken to be the same as in $FeBO_3$ [15], namely, $A = 3.42$ eV and $\varepsilon_d = -14.84$ eV.

The high intensity of absorption band *C* in the spectrum of $GdFe_3(BO_3)_4$ is explained, as in $FeBO_3$, by the superposition of an additional charge-transfer absorp-

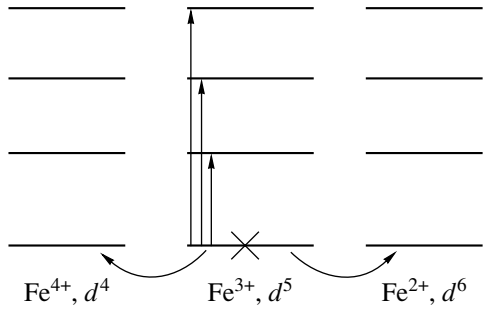

Fig. 3. Diagram of the Fe^{4+}, Fe^{3+}, and Fe^{2+} terms; the cross indicates the ground term $^6A_{1g}$, which is filled at $T = 0$.

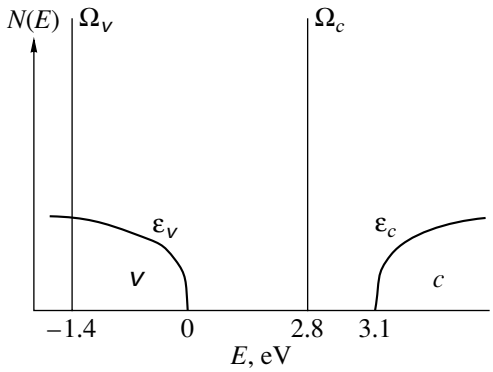

Fig. 4. Density of states of $GdFe_3(BO_3)_4$. The Fermi level lies above the valence band top ε_v.

tion mechanism, i.e., by the p^6d^5–p^5d^6 process. The creation of an excess electron due to the $Fe^{3+} \longrightarrow Fe^{2+}$ transition (Fig. 3) requires an energy

$$\Omega_c = E(^5T_2, d^6) - E(^6A_1, d^5). \quad (4)$$

Similarly, the annihilation of an electron is associated with the $Fe^{3+} \longrightarrow Fe^{4+}$ transition and requires an energy

$$\Omega_v = E(^6A_1, d^5) - E(^5E_1, d^4). \quad (5)$$

The levels Ω_c and Ω_v are expressed in terms of the Racah parameters as

$$\Omega_c = \varepsilon_d + 5A + 14B - 0.4\Delta, \quad (6)$$

$$\Omega_v = \varepsilon_d + 4A - 14B + 0.6\Delta; \quad (7)$$

and can be interpreted as the top and bottom Hubbard subbands. The difference between them determines the effective Hubbard parameter

$$U_{\text{eff}} = \Omega_c - \Omega_v = A + 28B - \Delta = 4.2 \text{ eV}. \quad (8)$$

This value of U_{eff} is typical of d ions in the middle of the 3d series. For example, this value of U_{eff} can be compared to the correlation energy $kT^* = 4.92$ eV, which was determined for crystal $Fe_{1.91}V_{0.09}BO_4$ from the temperature dependence of resistance using the Éfros–Shklovskiĭ law [17].

It should be noted that borates have different magnetic ordering temperatures ($T_{N1} = 38$ K for $GdFe_3(BO_3)_4$ and $T_{N2} = 348$ K for $FeBO_3$). The effect of magnetic order on the optical properties is different in the three temperature ranges: (i) below the magnetic ordering temperature, $T < T_{N1}$, the electronic structures of both borates are qualitatively similar but differ quantitatively due to the splitting of the A, B, and C bands in the molecular field, because their temperatures T_N differ by a factor of 10; (ii) in the range $T_{N1} < T < T_{N2}$, the electronic structures of borates should differ due to their magnetic properties being different; (iii) and in the paramagnetic phase, namely, at $T > T_{N2}$, the electronic structures of both borates are similar both qualitatively and quantitatively. The last conclusion is valid if there is no contribution from the Gd^{3+} f electrons, which appears only if the exciting energies are $\hbar\omega \approx 4$ eV or higher. For the same reason, substitution of neodymium for gadolinium causes additional lines to appear in the absorption spectrum and results in a more complicated electronic structure of the substituted crystals $Gd_{1-x}Nd_xFe_3(BO_3)_4$.

Taking into account all these considerations and the experimental data, we come to the model of the electronic structure of $GdFe_3(BO_3)_4$ shown in Fig. 4.

5. PROPERTIES OF $GdFe_3(BO_3)_4$ UNDER HIGH PRESSURES PREDICTED FROM THE MANY-ELECTRON MODEL

From the above discussion and calculations, as well as from the similarity between the electronic structures of $GdFe_3(BO_3)_4$ and $FeBO_3$, it follows that $GdFe_3(BO_3)_4$ will exhibit the following behavior: a crossover from the high-spin to low-spin state of the Fe^{3+} ion, collapse of the magnetic moment, a weakening of Coulomb correlations, an abrupt reduction in the energy gap, and an insulator–semiconductor transition.

According to [18], the effect of an increased pressure on the electronic structure is mainly due to an increase in the crystal field Δ:

$$\Delta(P) = \Delta(0) + \alpha P. \quad (9)$$

As a result, as can be seen from the Tanabe–Sugano diagrams for Fe^{3+} [19], the high-spin $^6A_1(S = 5/2)$ term and the low-spin $^2T_2(S = 1/2)$ term approach each other (Fig. 5a).

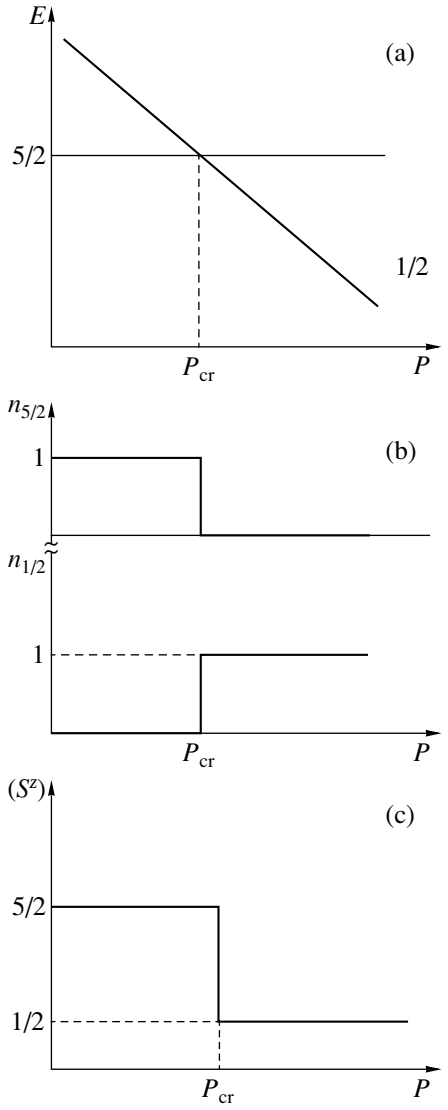

Fig. 5. (a) Fragment of the Tanabe–Sugano diagram for the crossover from the high-spin $^6A_1(S = 5/2)$ to low-spin $^2T_2(S = 1/2)$ iron terms, (b) the probability of an Fe^{3+} ion being in the $S = 5/2$ and 1/2 states, and (c) the collapse of the magnetic moment.

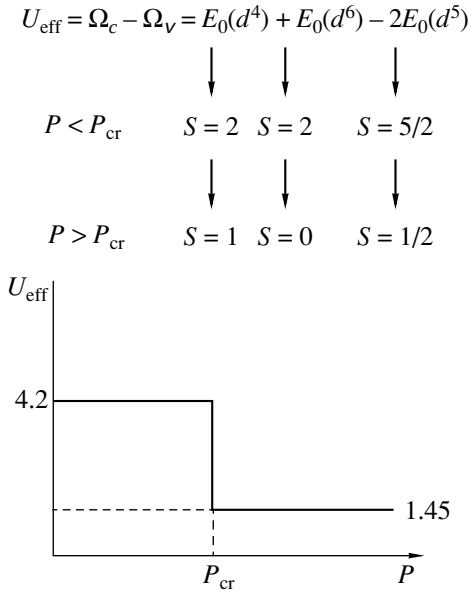

Fig. 6. Crossovers of terms for the d^4, d^5, and d^6 configurations and the jump in the effective Hubbard parameter.

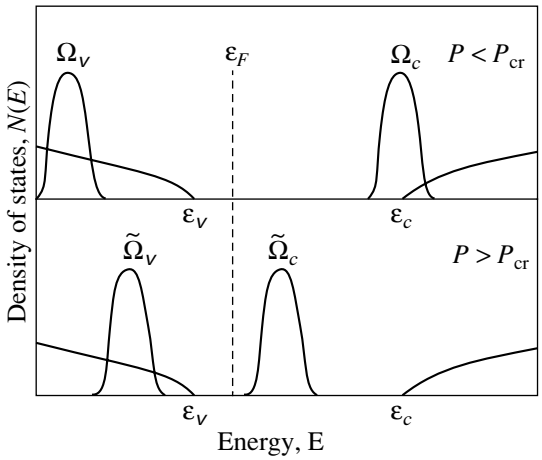

Fig. 7. $GdFe_3(BO_3)_4$ density of states under low and high pressure in the many-electron *p–d* model.

Therefore, at $P = P_{cr}$, the crossover can also occur in $GdFe_3(BO_3)_4$, which results in a collapse of the magnetic moment (Fig. 5b):

$$\langle S^z \rangle = 5/2 n_{5/2} + 1/2 n_{1/2}, \quad (10)$$

where $n_{5/2}$ and $n_{1/2}$ are the probabilities of the Fe^{3+} ion being in the $S = 5/2$ and $S = 1/2$ states, respectively. At $T = 0$, we have $n_{5/2} = 1$ up to the crossover point, and then this probability becomes zero above P_{cr}; the probability is $n_{1/2} = 0$ at $P < P_{cr}$ and $n_{1/2} = 1$ at $P > P_{cr}$.

For $FeBO_3$, the critical pressure P_{cr} is about 47 GPa [11]. For $GdFe_3(BO_3)_4$, a similar crossover can be expected and the critical pressure should have a similar value, because the Fe–O length and the critical field Δ are close to the respective values for $FeBO_3$. Under high pressure, the energies of the lower and the upper edges of Hubbard bands change due to the crossover [18]. We thus get for Fe^{3+}

$$\tilde{\Omega}_c = E(^1A_1, d^6) - E(^2T_2, d^5), \quad (11)$$

$$\tilde{\Omega}_v = E(^2T_2, d^5) - E(^3T_1, d^4). \quad (12)$$

As a result, the Hubbard effective correlation parameter decreases (Fig. 6), which means there is a decrease in the gap between the Hubbard subbands:

$$U_{eff} = \tilde{\Omega}_c - \tilde{\Omega}_v = A + 9B - 7C \approx 1.45 \text{ eV}. \quad (13)$$

A dramatic (almost threefold) decrease in SEC thus occurs, and instead of the Mott–Hubbard insulator we get the semiconductor state (Fig. 7).

A further increase in pressure can result in closure of the semiconductor gap (due to the increase in the small *d*-band width) and in the subsequent transition to the metal state.

6. CONCLUSIONS

The optical properties of the grown single crystals $GdFe_3(BO_3)_4$ and $GdFe_{2.1}Ga_{0.9}(BO_3)_4$ have been studied. It has been proved both theoretically and experimentally that, in the paramagnetic phase, the electronic structure and the optical spectra of $GdFe_3(BO_3)_4$ and $FeBO_3$ are similar to each other in the energy range below 4 eV in the vicinity of the Fermi energy. A many-electron model of the band structure of $GdFe_3(BO_3)_4$ has been suggested taking into account SEC of iron *d* states. It has been established that, under normal conditions, $GdFe_3(BO_3)_4$ is a charge-transfer insulator with SEC. In terms of the many-electron model, an increase in pressure was predicted to result in a crossover from the high-spin to low-spin state of the Fe^{3+} ion in $GdFe_3(BO_3)_4$, collapse of the magnetic moment, Coulomb correlation weakening, an abrupt reduction in the energy gap, and an insulator–semiconductor transition.

ACKNOWLEDGMENTS

This work was supported by the Russian Foundation for Basic Research (project no. 03-02-16268) and the program of the Department of Physical Sciences of the Russian Academy of Sciences "Strongly Correlated Electrons."

REFERENCES

1. N. I. Leonyuk and L. I. Leonyuk, Prog. Cryst. Growth Charact. **31**, 179 (1995).
2. A. D. Balaev, L. N. Bezmaternykh, I. A. Gudim, S. A. Kharlamova, S. G. Ovchinnikov, and V. L. Temerov, J. Magn. Magn. Mater. **258–259**, 532 (2003).
3. A. D. Balaev, L. N. Bezmaternykh, S. A. Kharlamova, V. L. Temerov, S. G. Ovchinnikov, and A. D. Vasi'ev, J. Magn. Magn. Mater. **286–287**, 332 (2003).
4. J. C. Joubert, T. Shirk, W. B. White, and R. Roy, Mater. Res. Bull. **3**, 671 (1968).
5. M. P. Petrov, G. A. Smolenskiĭ, A. P. Paugurt, S. A. Kizhaev, and M. K. Chizhov, Fiz. Tverd. Tela (Leningrad) **14**, 109 (1972) [Sov. Phys. Solid State **14**, 87 (1972)].
6. I. S. Édel'man, A. V. Malakhovskiĭ, T. I. Vasil'eva, and V. N. Seleznev, Fiz. Tverd. Tela (Leningrad) **14**, 2810 (1972) [Sov. Phys. Solid State **14**, 2442 (1972)].
7. A. V. Kimel, R. V. Pisarev, J. Hohlfeld, and Th. Rasing, Phys. Rev. Lett. **89**, 287401 (2002).
8. A. J. Kurtzig, R. Wolf, R. C. Le Graw, and J. W. Nielsen, Appl. Phys. Lett. **14**, 350 (1969).
9. N. F. Mott, Proc. Phys. Soc. A **62**, 416 (1949).
10. A. G. Gavriliuk, I. A. Trojan, R. Boehler, M. Eremets, A. Zerr, I. S. Lyubutin, and V. A. Sarkisyan, Pis'ma Zh. Éksp. Teor. Fiz. **75** (1), 25 (2002) [JETP Lett. **75**, 23 (2002)].
11. I. A. Troyan, M. I. Eremets, A. G. Gavrilyuk, I. S. Lyubutin, and V. A. Sarkisyan, Pis'ma Zh. Éksp. Teor. Fiz. **78** (1), 16 (2003) [JETP Lett. **78**, 13 (2003)].
12. V. A. Sarkisyan, I. A. Troyan, I. S. Lyubutin, A. G. Gavrilyuk, and A. F. Kashuba, Pis'ma Zh. Éksp. Teor. Fiz. **76** (11), 788 (2002) [JETP Lett. **76**, 664 (2002)].
13. L. N. Bezmaternykh, S. A. Kharlamova, and V. L. Temerov, Crystallogr. Rep. **49**, 855 (2004).
14. E. P. Chukalina, D. Yu. Kuritsin, M. N. Popova, L. N. Bezmaternyhk, S. A. Kharlamova, and V. L. Temerov, Phys. Lett. A **322**, 239 (2004).
15. S. G. Ovchinnikov and V. N. Zabluda, Zh. Éksp. Teor. Fiz. **125**, 198 (2004) [JETP **98**, 135 (2004)].
16. D. T. Sviridov, R. K. Sviridova, and Yu. F. Smirnov, *Optical Spectra of Transition Metal Ions in Crystals* (Nauka, Moscow, 1976) [in Russian].
17. A. D. Balaev, O. A. Bayukov, A. D. Vasil'ev, D. A. Velikanov, N. B. Ivanova, N. V. Kazak, S. G. Ovchinnikov, A. Abd-Elmeguid, and V. V. Rudenko, Zh. Éksp. Teor. Fiz. **124** (5), 1103 (2003) [JETP **97**, 989 (2003)].
18. S. G. Ovchinnikov, Pis'ma Zh. Éksp. Teor. Fiz. **77**, 808 (2003) [JETP Lett. **77**, 676 (2003)].
19. Y. Tanabe and S. Sugano, J. Phys. Soc. Jpn. **9**, 753 (1951).

Translated by E. Borisenko